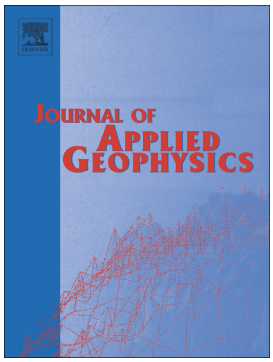

An overview of non-destructive and minimally invasive techniques for moisture control in the cultural heritage

M.I. Martínez-Garrido, R. Fort, M. Gómez-Heras, J. Valles-Iriso, M.J. Varas-Muriel

PII: S0926-9851(17)30438-X
DOI: doi:10.1016/j.jappgeo.2018.03.008
Reference: APPGEO 3466

To appear in:

Received date: 3 May 2017
Revised date: 9 March 2018
Accepted date: 13 March 2018

Please cite this article as: M.I. Martínez-Garrido, R. Fort, M. Gómez-Heras, J. Valles-Iriso, M.J. Varas-Muriel , An overview of non-destructive and minimally invasive techniques for moisture control in the cultural heritage. The address for the corresponding author was captured as affiliation for all authors. Please check if appropriate. Appgeo(2017), doi:10.1016/j.jappgeo.2018.03.008

AN OVERVIEW OF NON-DESTRUCTIVE AND MINIMALLY INVASIVE TECHNIQUES FOR MOISTURE CONTROL IN THE CULTURAL HERITAGE

M.I. Martínez-Garrido[1], R. Fort[1], M. Gómez-Heras[1,2], J. Valles-Iriso[3], M.J. Varas-Muriel[1,4]

[1] Instituto de Geociencias IGEO (CSIC, UCM), C/José Antonio Nováis 12, 28040, Madrid, Spain

[2] Departamento de Geología y Geoquímica, Universidad Autónoma de Madrid, Madrid, 28049, Spain

[3] Centro de Asistencia a la Investigación de Arqueometría y Análisis Arqueológico (UCM), C/ Profesor Aranguren, s/n, 28040, Madrid, Spain

[4] Facultad Ciencias Geológicas, Universidad Complutense de Madrid (UCM), C/José Antonio Nováis 12, 28040, Madrid, Spain

ABSTRACT

This article describes the use of non- or minimally destructive methods to study damp in San Juan Bautista Church at Talamanca de Jarama in the Spanish province of Madrid. The combination of ground penetrating radar (GPR), electrical resistivity tomography (ERT) and wireless sensor network (WSN) techniques provided sub-surface information, while data on wall surfaces were collected with contact hygrometry and infrared thermography. The respective findings and ranges of observation were inter-related to identify the decay associated with the damp and determine the advantages and drawbacks of each instrumental method.

1. INTRODUCTION

Monitoring involves observing one or several parameters to detect possible anomalies in need of ongoing surveillance [1]. With the development of innovative detection techniques, its use has extended to a growing number of fields. Monitoring systems often comprise several types of sensors [2, 3] and instrumentation based on electrical resistivity [4, 5], wave propagation [6-8] or infrared radiation [9, 10], among others.

Many cultural heritage studies conclude with recommendations on monitoring the risks to which a cultural heritage asset may be subject as part of a preventive conservation strategy or to avert or minimise damage [11-13]. With the use of non-destructive or minimally invasive techniques [14], damage can be detected in an incipient stage and specific action can be taken. This enhances asset maintenance, preventing the decay or loss of emblematic structures or the need for costly and extensive restoration [1].

As studies on damp in historic buildings are normally based on a single instrumental technique [15-18], comparison among the various options to determine which is the most effective is not straightforward. This study aimed to develop a method for monitoring damp on the walls of a specific building with a view to its more general application to the built heritage. The case study was conducted on San Juan Bautista Church at Talamanca de Jarama, a town in the Spanish province of Madrid. A number of non-destructive or minimally invasive techniques were used to determine the source of the damp on its walls, as well as any inter-wall differences associated with orientation or composition. The ultimate aim was to propose preventive action and formulate conservation guidelines. The approach is applicable to any structure exposed to this type of decay. A comparison was drawn to determine the applicability of each technique to studies on the causes of decay in the architectural heritage.

2. METHODS

The study objectives were pursued with several non-invasive monitoring instruments, including data loggers, electrical conductivity and resistivity meters, infrared thermographic cameras and ground-penetrating radar antennas.

This section describes the study scenario, along with the techniques and deployment schemes used. The building analysed in the case study was chosen in light of the intense damp of uncertain origin present in its walls. As several possible sources of the problem were considered, including indoor variability, leakage, the rise of capillary water and the type of construction material used, monitoring techniques based on different physical principles (such as resistivity or wave propagation) were used at different depth ranges.

2.1. SCENARIO

San Juan Bautista Church, located at Talamanca de Jarama in the Spanish province of Madrid, measures 36.50 m long by 12.70 m wide and 10.50 m high. It was listed as an historic-artistic monument on 3 June 1931. When this Romanesque church was built in the twelfth to thirteenth centuries, it had a single nave. Its dolostone apse is the sole part of the original building that has been conserved [19], for the nave was demolished in the sixteenth century and rebuilt to Renaissance aesthetics. Two side aisles were also constructed, with large arches that rest on sturdy columns with richly decorated capitals and support a Mudejar-style ceiling. The Baroque bell tower was built with limestone ashlars between the seventeenth and eighteenth centuries [20].

The dolostone ashlars on the church apse, its two entrance portals and the indoor columns were quarried locally [19, 21]. From the sixteenth century on, the construction materials used in San Juan Bautista Church were primarily dolostone rubble masonry and ashlars, mortar, brick and clay filler.

The church stands 0.4 m to 0.5 m below street level, with its south-east entrance facing a spacious square.

Its north (Figure 1c) and south (Figure 1a) perimetric walls are severely affected by damp, visible mainly from indoors around the west entrance (Figures 1b and 1d).

Figure 1. a) South façade of the church showing the indoor area studied from the outside; b) indoor south wall near the confessional alongside the main (west) entrance; c) north façade showing the indoor area studied from the outside; d) detail of damp on indoor wall

The areas studied were located on the west end of the north (Figure 1c)) and south (Figure 1a)) walls. They were chosen after being identified as the sites most severely affected by damp preliminary by in-wall, long-term monitoring using wireless sensor networks [22] and microclimatic studies based on data logger readings [20, 23] (Figures 1b) and 1d)). The severity of the problem was governed by the type of construction materials and procedures [19], outdoor climate and the steep variations in the indoor microclimate attendant upon the use of heating in winter and its effect on the conservation of church interiors [19, 20, 23].

The north and south walls, both 0.6 m wide, are made of dolostone and quartzite ashlars and rubble masonry, brick and joint and surface mortars. On the south façade, bricks laid with lime mortar surround panes of dolostone rubble masonry. At the base is has an 0.8 m high dado made with the same dolostone rubble masonry (Figure 1a)). These same materials are found on the north façade, although laid in a less orderly fashion (Figure 1c)). Two types of brick masonry were used: on the upper part of the wall, brick flanks large whitewashed panes, whilst at intermediate heights it flanks smaller panes where much more mortar was used to receive the dolostone rubble masonry and quartzite

pebbles. Mortar surfacing and quartzite pebble masonry are particularly prevalent on the northwest corner of the north wall. The base of this wall to a height of 0.6 m is made of dolostone rubble masonry and ashlars. Indoors, these walls have multi-layer rendering around 0.10 m thick which from the outside in consists in paint, a 0.03 m layer of lime mortar or plaster and a clay filler reinforced with brick and rock fragments. The base of the walls to a height of 1.0 m to 1.2 m have a cement mortar layer up to 0.05 m thick between the lime mortar or plaster and the clay filler.

2.2. ASSESSMENT TECHNIQUES

Cultural heritage buildings in general and the building studied in particular are characterised by different construction materials with varying performance that may well lead to very different types of decay under the same environmental conditions. Reconstruction and refurbishment must therefore be preceded by relative humidity (RH) and temperature (T) monitoring, as well as by material identification and differentiation (see section 2.1) to correctly determine the main causes of decay. Damp-related decay has a number of origins, ranging from capillary water absorption to leakage and condensation. A detailed study of these origins requires the combined use of different techniques.

The non- or minimally invasive techniques used in this study are diagrammed in Figure 2.

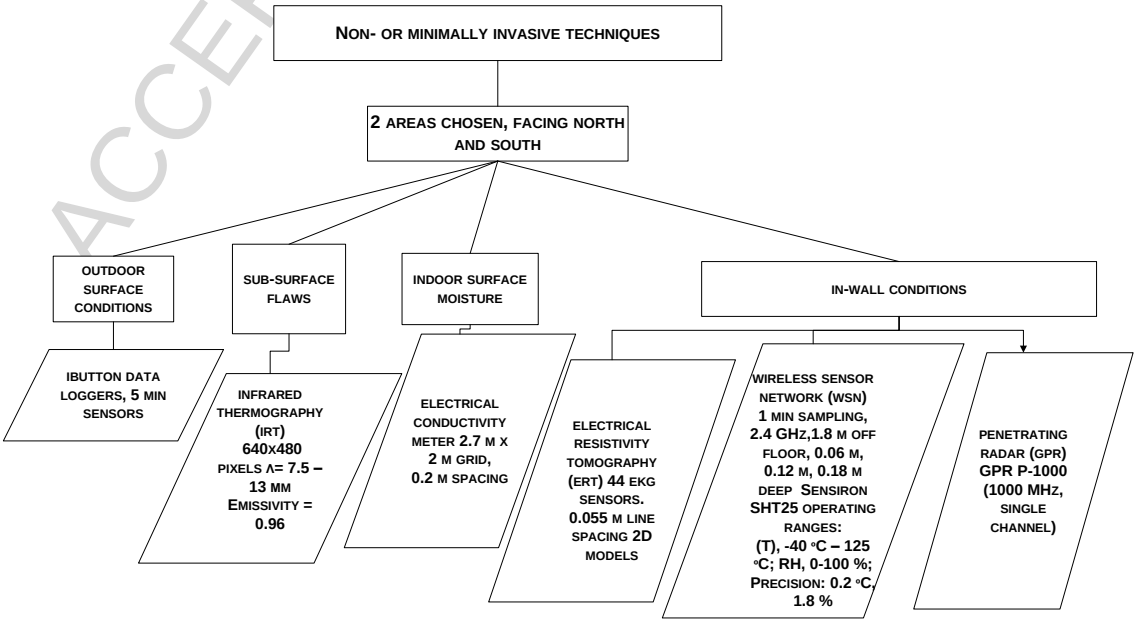

Figure 2. Techniques for monitoring and studying damp

2.2.1. ELECTRICAL CONDUCTIVITY METER

Wall surface damp was measured with a General Electric Protimeter Surveymaster electrical conductivity meter that determined surface moisture based on the electrical resistivity between two pins nailed to the wall at 0.0135 m from one another [24]. This instrument measured moisture content from 7 % to 99 % of wood moisture equivalent (%WME). Although designed specifically for wood, these meters are widely used for comparative estimates of the degree of moisture in surfaces with a variety of construction materials (such as plaster, cement and stone). [22, 25]. The distribution of the moisture content in the areas studied was mapped with SURFER software [26]. Readings were taken on a grid with points spaced at 0.2 m intervals over an area measuring 2.5 m to 2.7 m high by 2.2 m wide.

2.2.2. INFRARED THERMOGRAPHY

The apparent temperature distribution in the areas of the walls studied was determined with a FLIR ThermaCAM B4 infrared thermographic camera (detection range 7.5 μm to 13 μm and 640 x 480 pixel resolution). Infrared thermography, while measuring the apparent surface temperature, can also furnish information on masonry substrates with plaster or mortar rendering, given the differing thermal properties of the two materials. A qualitative survey was conducted on the walls analysed here. Inasmuch as the aim of the thermographic review in this case was to characterise the masonry underneath the rendering, no correction was made for temperature, relative humidity or distance and a common fixed emissivity value of 0.96 was defined for all the construction materials [18]. The images were recorded after heating the church for 30 minutes to enhance the thermal contrast between the materials.

2.2.3. SENSORS: DATA LOGGERS AND WIRELESS SENSOR NETWORKS

a) Data loggers

Since the monitoring time was relatively short and the acquisition rate (every 5 min) not especially demanding, iButton DS1923 data loggers [27] were deemed to

suffice to record conditions on the two façade exteriors. These 16.3 mm diameter, 5.0 mm high devices feature an 8 bit resolution and an operating range for T of -20 °C to 85 °C (precision, ±0.5 °C) and for RH of 0 % to 100 % (precision, ±0.6 %) The sensors were programmed and the data downloaded with iButton 1-Wire Viewer software [28].

b) Wireless sensor networks (WSN)

The information on apparent temperature distribution (°C) and relative moisture values (%WME) obtained was used to install wireless sensors inside the two walls at depths of 0.06 m, 0.12 m and 0.18 m to establish in-wall T and RH. SmartmoteWS version 3.21 sensor nodes or motes were positioned at 1.8 m off the floor and used with a Smartmote version 3.20 base station (Figure 3) [29]. These motes had four inter-integrated circuit (I2C) T/RH input ports, a 2.4 GHz radio transceiver and 8.5 Ah, 3.6 V ER26500 lithium batteries. They operate to a tree-type communications topology [30-32]. On the grounds of the 100 % success rate for received messages found for this wireless platform in a wireless communications study [33], it was chosen over other platforms [34]. The motes, fitted with IP65-rated bodies [35], can operate within a temperature range of -25 °C to 85 °C, whereas the Sensiron SHT25 T/RH sensors used in the Smartmote network had an operating range of -40 °C to 125 °C.

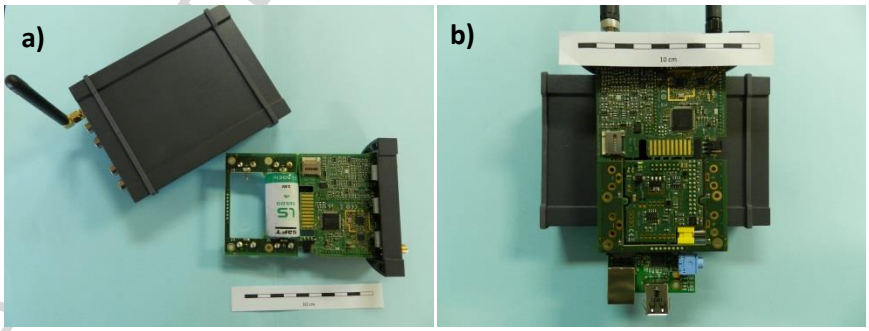

Figure 3. a) Version 3.21 mote and b) version 3.20 base station for the Smartmote platform

2.2.4. ELECTRICAL RESISTIVITY TOMOGRAPHY (ERT)

Electrical resistivity tomographic measurements were taken on the north and south walls using the Wenner [36] technique and a Geolog2000 GeoTom device [37]. In the Wenner method a current is run through two outer electrodes and the difference in

potential between the two inner electrodes is measured. Resistivity is then calculated from Ohm's law from the following equation:

$$\rho = \frac{2\pi aV}{I} \quad (1)$$

where ρ is apparent resistivity, *a* is the distance between electrodes, *V* the difference in potential between the two inner electrodes and *I* the current applied to the outer electrodes. The current applied to the electrodes is varied at each measuring point in the cross-section until a reading for *V* is obtained. The cross-sections obtained taper depth-wise, for the greater the distance between the outer electrodes the smaller is the number of measurements. A line of 44 electrocardiogram (EKG) electrode sensors spaced at 0.055 m was used to obtain two-dimensional cross-sections for the survey [25]. All abnormally high or low values were purged from the apparent resistivity dataset acquired. An apparent resistivity pseudo-cross-section was found with least squares inversion, reiterating until the difference between two consecutive inversion values was under 5 %.

Two profiles were defined: one as a vertical line along the indoor wall and the other perpendicular to it along the floor, with the lower end of the wall profile intersecting with the centre of the floor profile.

2.2.5. GROUND-PENETRATING RADAR (GPR)

GPR has become particularly popular in heritage research in recent years to detect heritage elements at archaeological sites [38-41] or structural damage [6, 7, 42-45] or other types of decay [42, 43, 46-48], including damp [49], in cathedrals.

A number of cross-sections of indoor walls and nearby indoor floors were monitored with GPR in the areas chosen for the study to gather information on in-wall conditions at greater depth ranges than reached in this study with the ERT and WSN techniques discussed earlier.

A US Radar Inc. P-1000 GPR [50] 1000 MHz antenna was used to obtain high resolution images to penetration depths of approximately one metre (in concrete). An electromagnetic pulse duration of 4 ns was applied with a 15 ns window.

This technique indirectly revealed the underlying structure in the walls and floors via the transmission of electromagnetic signals and the subsequent reception of the reflections generated by the discontinuities present. In physical terms, the technique is sensitive to all variations in electrical conductivity and permittivity as well as magnetic permeability to be found in a medium, whether due to lithological changes or the presence of objects [51, 52].

Three horizontal (parallel to the floor, see Figures 4a) and 4b), above) survey profiles were defined at heights of 0.1 m, 1.0 m and 2.0 m and a total of 10 vertical profiles at intervals of approximately 0.5 m (Figures 4a) and 4b), above).

In the floor areas, three survey profiles each were recorded parallel to the south (Figure 4a), below) and north (Figure 4b), below) walls. A profile perpendicular to the south wall was also defined (Figure 4a, bottom). Profile nomenclature is shown in Figure 4.

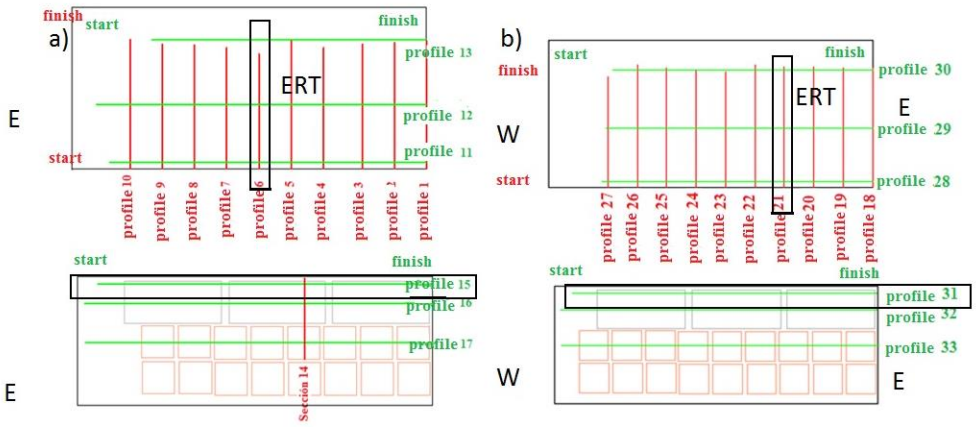

Figure 4. GPR survey profiles in a) south-side wall (above, elevation view) and floor (below, plan view); b) north-side wall (above, elevation view) and floor (below, plan view); solid black outline: profiles where ERT was also performed

Several electromagnetic wave processing criteria (gain adjustments, frequency filters) were applied to the radargrams using the 2D and 3D versions of GPR SLICE V7.0

software. This software features filtering algorithms to post-process the data. The images were processed by 'dewowing', plotting with automatic gain control (AGC) gain and applying bandpass 200-1100 and background removal filtering, assuming a velocity of 0.095 m/s for all the wall layers.

3. RESULTS

3.1. ELECTRICAL CONDUCTIVITY METER

Electrical conductivity meter readings were regarded as essential to determine damp distribution on the church walls. The technique was likewise imperative for defining the positions of the points on the wireless sensor network used to record long-term T and RH fluctuations [22], for it detected the most intense moisture fronts. This information was needed to delimit the area studied, at, above and below each front. The results delivered by this technique were primarily applicable to the plaster and lime and cement mortar on the indoor walls of the church, which often mirrored the moisture content in the rest of the in-wall materials.

Monitoring campaigns were conducted in July and November 2011, March 2012 and February 2014 to compare the moisture front fluctuations to the variations in outdoor weather conditions in different seasons of the year. Surface moisture readings were recorded on the indoor walls in the areas affected by damp on the east and west sides of the north and south façades of the church.

In both the 2011 and 2012 campaigns, a moisture front was detected at around 1.5 m off the floor in the southwest area in summer, autumn and winter, with WME values of over 75 % that intensified to over 90 % with rainfall in autumn and snowfall in winter. The area below 0.5 m exhibited a less uniform distribution of moisture, in which areas with surface %WMEs of up to 90 % were interspersed with areas with values ranging from 45 % to 75 %. A similar distribution was found for the southeast wall, where the moisture front was located at a height of around 1.0 m, although the values in the lower wall were not as high as on the southwest wall, which was more visibly affected by surface damp.

The highest WME values in the northwest, in turn, were found at heights of under 0.5 m, where saturation (>90 % WME) was recorded. Readings of over 75 % were recorded in the areas higher than 0.5 m, primarily during autumn rains and winter rain/snow. The values found in the east end of the north wall in the summer were <45 % WME, which in the autumn tended to rise to 90 % WME at heights of under 1.0 m.

As noted earlier, the distribution of these electrical conductivity meter data provided the grounds for positioning the points in a wireless sensor network for long-term, in-wall monitoring [22].

Wintertime readings were repeated on 18 February 2014 in the areas most severely affected (west end of the south (Figure 5a)) and north (Figure 5b)) walls). The findings revealed a similar distribution of WME values by area and height, confirming the persistence and pattern of the damp problems detected. Further to these findings, the study areas chosen were the north and south walls around the west entrance. Figure 5 shows the hygrometric results of readings taken on the same day in those two areas. Note the high %WME values on the northwest wall, possibly due to capillary water rise, where problems associated with the stone dado on the southwest wall were also observed.

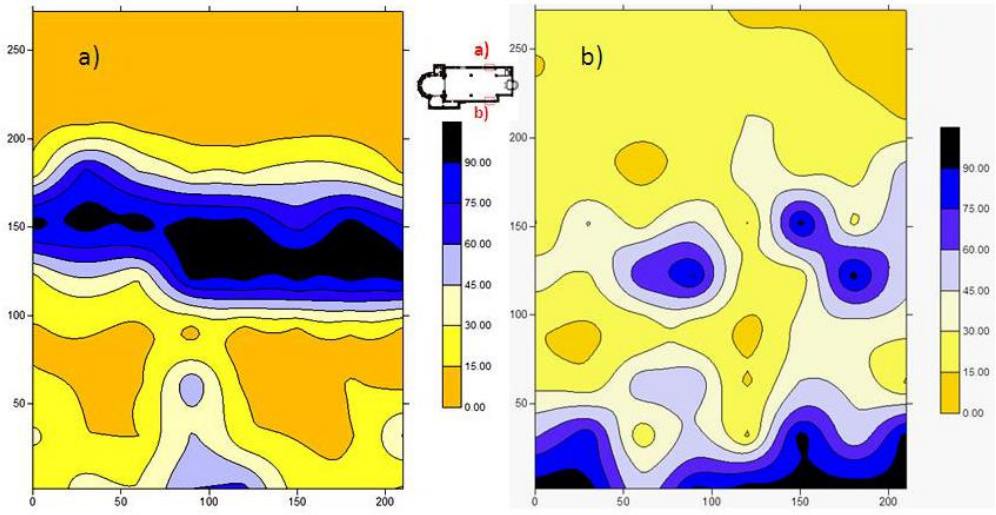

Figure 5. Results of electrical conductivity meter readings taken on 18 February 2014 a) on the southwest wall; and b) on the northwest wall of the church [x-axis: (cm); y-axis: (cm); colour scale: %WME]

3.2. INFRARED THERMOGRAPHY

The infrared thermographic studies conducted in the church supplemented the electrical conductivity findings. This technique also distinguished the construction layers in the walls and hence the construction materials used.

The lower apparent surface temperature in the underside than in the rest of the north wall (Figure 6a)) was attributed to two factors: its different masonry and a moisture front that reached a height of 1.0 m to 1.5 m. Surface temperature was highest at approximately 1.5 m off the floor in an area that warmed more quickly with the heating, for its rendering had fallen away, lowering its thermal mass. The change in wall masonry visible on the left in Figure 6a) (west), near the foot of the church, identifies the area where the façade consists in small rubblestone panels flanked by brick. In the rest of the wall, the stone dado at the base can be clearly distinguished from the upper brick masonry. As the thermographic images of the interior and exterior wall around the crucifix (Figures 6a) and 6b, respectively) show, the masonry substrate under the indoor rendering was not the same as in the exterior wythe. The indoor image also revealed a number of thermal anomalies on the surface attributed to rainwater leaks through a crack and the shrinkage joint between the rubble masonry and the brick wall. The layers comprising these wythes and the inward extent of the leakage were studied with ERT and GPR.

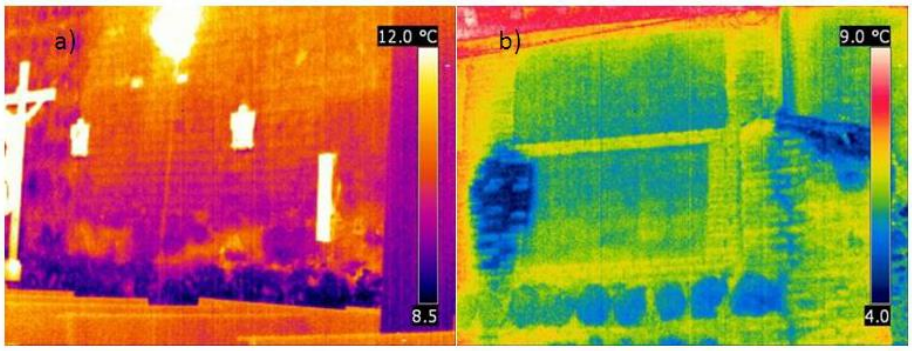

Figure 6. Infrared thermographs taken on 18 February 2014 of a) the indoor north wall after heating the church for 30 minutes; and b) the outdoor north wall at around midday

The aforementioned findings were applied to establish the conditions for using other techniques in this area. Thermographic surveys conducted in conjunction with electrical resistivity trials [25] on 24 March 2014 (see section 3.4) showed that the range of apparent temperature fluctuation was narrower on the north than on the south wall, where differential behaviour was detected in the most severely decayed areas, at 1.0 m to

1.8 m off the floor. The thermographic findings for the north wall also identified the areas where damp was greatest in the shallowest layers (plaster or lime mortar, spalling), at heights of 0.9 m to 1.3 m.

Thermography confirmed the existence in the south wall of a moisture front at around 1.5 m off the floor, with areas severely affected by damp under 0.5 m.

3.3. SENSORS: DATA LOGGERS AND WIRELESS SENSOR NETWORKS

The iButton DS1923 data loggers positioned on church exteriors, together with the Smartmote wireless sensor network deployed indoors, respectively delivered outdoor T and RH and in-wall data at a height of 1.8 m and depths of 0.06 m, 0.12 m and 0.18 m. Conditions were monitored on 24 March 2014 from 11.30 h to 14.00 h in parallel with the electrical resistivity inspections. The mean outdoor readings were T=12.0 °C and RH=65.4 % on the north façade and T=21.8 °C and RH= 36.5 % on the south façade. The effect of solar radiation was clearly visible in these mean values, with substantially higher mean temperature and lower mean relative humidity on the south than on the north wall.

Figure 7 shows the Smartmote wireless sensor network findings for T and RH inside the wall. Relative humidity values were close to saturation in the north wall, with severe damp in the upper levels. A temperature gradient was observed, with values tending to rise slightly in the inward direction. The temperature gradient in the south wall followed the opposite pattern, with the highest temperatures in church exteriors. Surface temperatures were slightly higher and less variable in the southwest than in the northwest. In-wall relative humidity on the south side rose with increasing depth in the outward direction.

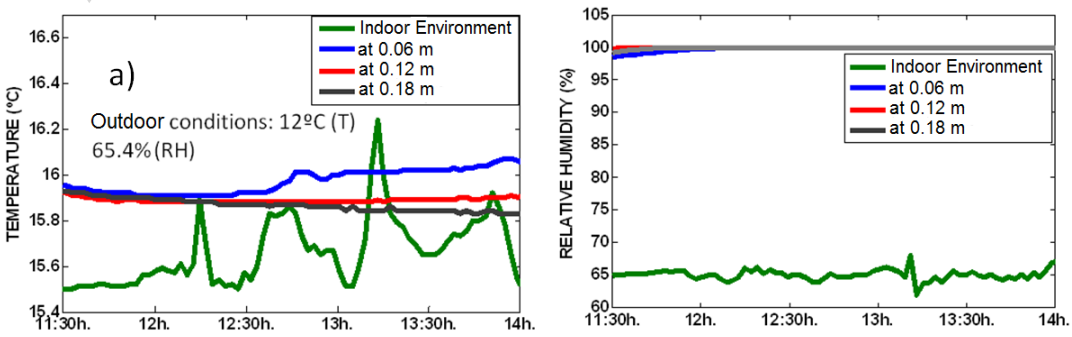

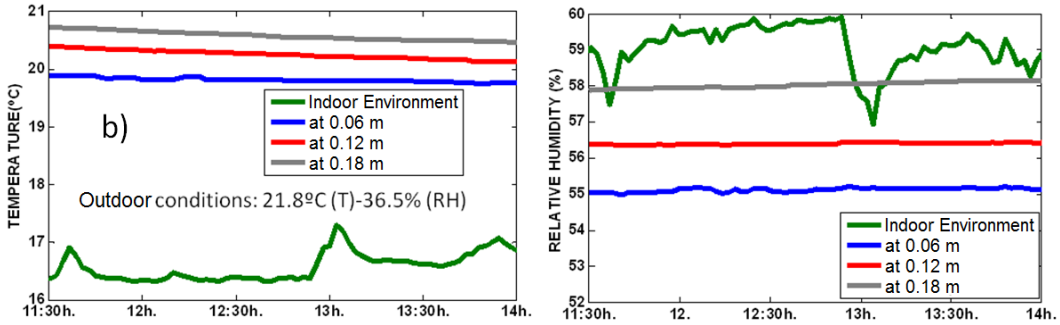

Figure 7. Smartmote WSN temperature and relative humidity curves at a height of 1.8 m and in-wall depths of 0.06 m, 0.12 m and 0.18 m for a) the north wall and b) the south wall

3.4. ELECTRICAL RESISTIVITY TOMOGRAPHY

After the aforementioned results were collected, electrical resistivity tomography was performed to obtain a multi-point, in-depth view of the walls, in keeping with the methods described in item 2.2.4.

The vertical line of profile positions was defined to include the points with the highest electrical conductivity meter readings (%WME) [25].

In the cross-section for the southwest wall (Figure 8a)), the highest apparent resistivity values (>236087 Ω), possibly denoting low moisture, were found above 1.0 m and below 0.2 m off the floor. Moreover, several ranges of resistivity values were detected. In the shallowest layer, to a depth of 0.16 m, resistivity varied with height, with lower apparent values (<113 Ω) over around 1.0 m, which were associated with a higher relative moisture content. That finding confirmed the presence of the moisture front detected with the electrical conductivity meter. A threshold height at 1.0 m to 1.2 m was also observed, with resistivity values in the intermediate range (113 -776 Ω) below it and in the low range (interpreted to denote higher moisture) above it. The exception was a thin horizontal layer just over 1.2 m that concurred with the moisture front detected with the electrical conductivity meter, where apparent resistivity was lowest (<16.8 Ω, denoting maximum moisture, salts or both).

The study conducted on the floor on the southwest side of the church (Figure 8b)) showed substantially lower apparent resistivities than the vertical cross-section, with

maxima of around 200 Ω, indicating that the moisture or salt content or both was generally higher than in the wall. This cross-section also revealed the presence of a surface layer with a higher moisture content (lower electrical resistivity, ≈14.8 Ω) and two large areas with values upward of 119 Ω and depths greater than 0.2 m, interpreted to be a tomb in light of their morphology and the context. Since the floor had such low resistivity, particularly where its outer surface abuts with the wall, and intermediate values (24.8 Ω - 41.9 Ω) at depths of 1.6 m to 2.0 m, the origin of the damp in this case was interpreted to be capillary water rising from the subsoil. That effect would be intensified by surface water, inasmuch as the church stands below street level and is flanked by a slightly downward sloping outdoor pavement.

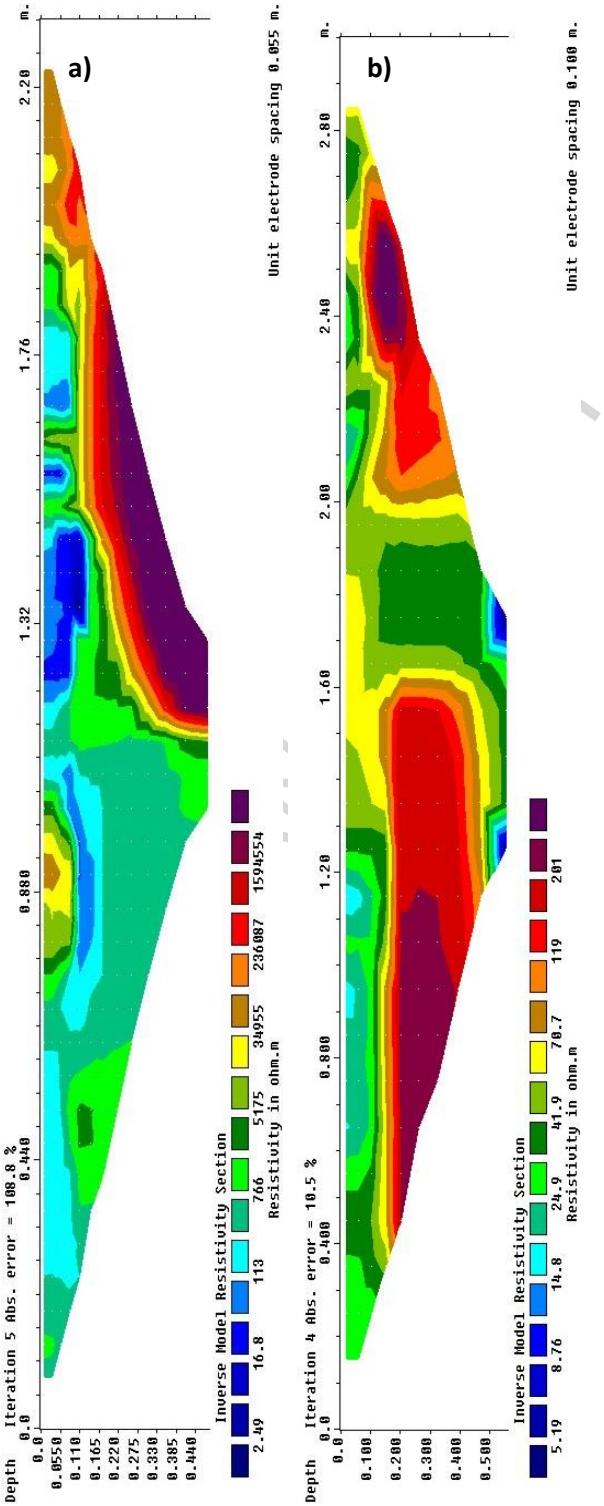

Figure 8. GeoTom profiles in the southwest a) wall; and b) floor of the church

On the north wall, in turn (Figure 9a)), the moisture content was observed to be high (≈300 Ω) in the medium-high part of the wall, at heights greater than 0.88 m (y-axis). This moisture (low resistivity) persisted up to a depth of 0.22 m (x-axis) across the entire vertical profile and up to 0.44 m at around mid-height (1.0 m to 1.3 m). The resistivity gradient was indicative of a predominant downward flow of moisture from the upper part of the wall, for the moisture content was lower in the mid-low heights, with resistivity values of over 851 Ω. Nonetheless, moisture peaks (resistivity nadirs) were detected in the shallowest areas on the lower wall (at a height of around 0.3 m and depth of around 0.11 m and a height of 0.6 m and depth of 0.05 m), along with moisture nadirs (resistivity peaks) likewise near the surface at higher elevations (height of 0.7 m and depth of 0.30 m).

As in the south cross-section (Figure 8), resistivity values were found to be generally lower in the floor than in the wall. That the lowest resistivity (highest moisture) values were not found in the shallowest layers along the wall-floor joint (Figure 9b)) provided further support for hypothetical rainwater leakage in the upper part of the wall as the origin of the damp. Nonetheless, low resistivity (< 62 Ω) was also observed at depths of up to 0.20 m, interspersed with areas of very low resistivity (<29 Ω). The highest resistivities (>133 Ω) were recorded at the greatest depths (>0.33 m), perhaps due to the presence of tombs. This somewhat higher resistivity area appeared to persist across the greatest depth studied, contrary to what was observed for the south-side floor, where low resistivity areas (0.45 m deep, resistivities <41.9 Ω) were observed to be interspersed, due in all likelihood to the presence of filler materials that would favour capillary water absorption in that wall.

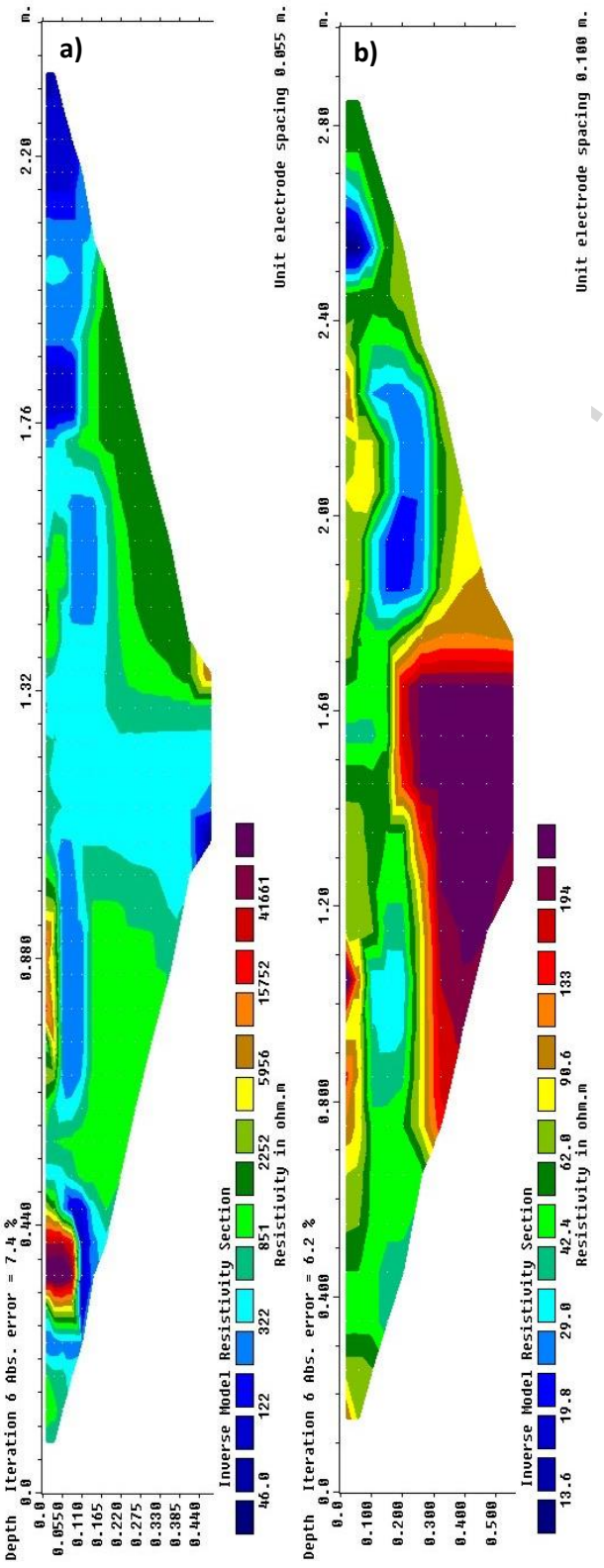

Figure 9. GeoTom profiles in the northwest a) wall; and b) floor of the church

3.5. GROUND PENETRATING RADAR

The GPR readings for this study were taken on 22 April 2014. Of the many cross-sections generated in the field study, this paper discusses only the ones that have a bearing on the other techniques deployed. The x-axis of the radargrams represents the distance in metres of antenna travel in the direction described in item 2.2.5, from the starting to the end point on the survey profile: height-wise on the wall and width-wise on the floor. The profile or bandpass number across which the 1000 MHz travelled is specified on each radargram. The right-hand scale on the y-axis represents the delay between the time the pulse was emitted by the source and the time the echo or reflection was detected by the receiver (as both are on the surface, this is the time needed for the wave to travel twice the distance to the target, known as two-way travel time in ns) [53], while the left-hand scale on the y-axis represents the depth of penetration inside the wall. The qualitative colour scale on the right represents the amplitude of the received wave.

a) South wall, vertical cross-sections

The most representative vertical cross-sections (profiles 1, 2, 4, 6 and 9 in Figure 4a)) on the south wall, including the vertical cross-section or radargram that concurred with the ERT profile (\bandpass\6), are shown in Figure 10.

The GPR findings for that wall detected a change in medium at a height of around 0.9 m to 1.0 m, which concurred with the height of the dado, above and below which clear differences were observed. The purple areas in these radargrams are indicative of the thickness of the plaster and cement mortar, in which a strip of a thinner layer of plaster is also visible. The blue line in Figure 10 represents the street level: the part of the cross-section lying to the right of that line was located above street level.

GPR confirmed the presence of moisture at heights of approximately 1.0 m to 1.5 m (red outline in Figure 10), where electrical resistivity values were very low (< 20 Ω) in the shallowest layers. Reflections were barely received in this area at any depth. Although according to the ERT findings, moisture at these heights declined substantially in the deeper layers (>0.10 m, >766 Ω), GPR recorded scant reflections in that height range across the entire thickness of the wall (Figure 10). That finding was attributable to

the moisture in the surface-most layers in the wave path, which slowed its velocity, inducing a loss of energy and perhaps adversely affecting the reliability of the results.

The vertical radargrams for this south wall also showed a series of greater reflections at heights of over 1.5 m (see black line in bandpass\6, Figure 10) which, in the absence of medium differences, were interpreted as lower moisture content. That concurred with the high electrical resistivity and low humidity (Figure 8a)) found with ERT, possibly reflecting the effect of solar radiation. In other words, whilst moisture (resistivities ≈100 Ω, Figure 8a)) was present in the shallowest layers, its impact on the cement mortar and hence on wave attenuation was lower, from which it may be surmised that even in the presence of moisture in shallow layers, GPR can detect lower moisture in layers at greater depths.

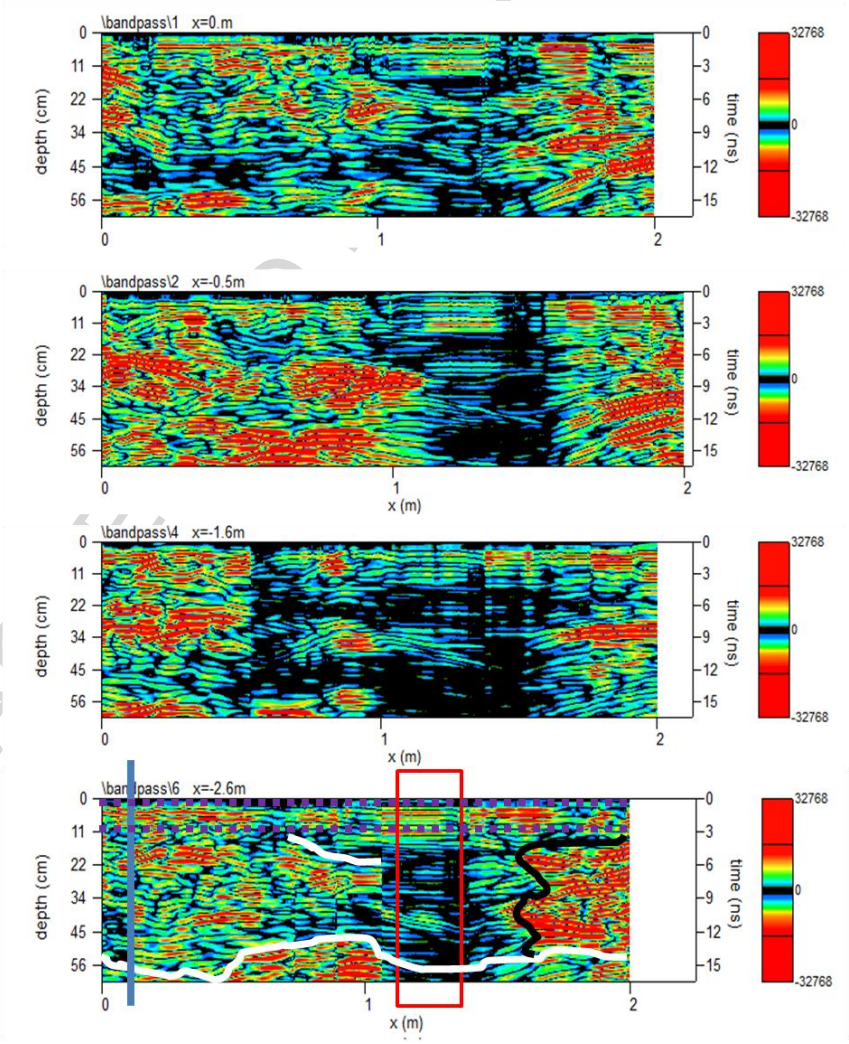

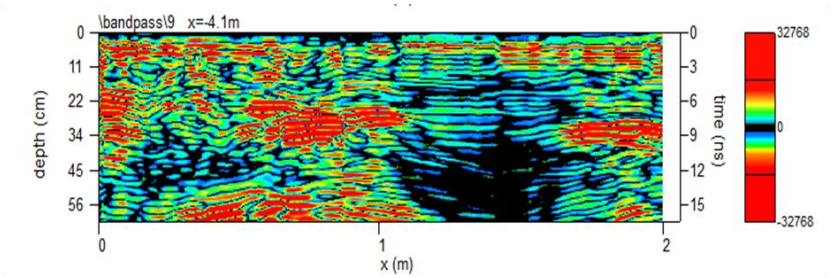

Figure 10. Radargram for the vertical survey profile that coincided with the electrical resistivity profile on the south wall; solid red outline: areas with scant reflections indicative of high moisture content; dashed purple outline: plaster and cement mortar layers; solid blue line: street level; solid white line: characteristic reflections or reflections for outside surface of wall; solid black line: lower boundary of area affected by solar radiation.

The wave reflections that identify the outside surface of the wall were observed to be delayed in the dado area at around 0.5 m and the upper wall at around 1.5 m to 1.7 m (white line, bandpass\6, Figure 10). That delay was associated with the moisture content detected in the shallow layers by ERT, where resistivities on the order of 100 Ω were recorded. New reflections (white line, bandpass\6, Figure 10) appeared at a height of around 1.0 m in the shallowest 0.20 m of the wall, possibly due to the presence of moister layers underneath dryer, shallower layers, as observed with ERT (Figure 8a)).

Amplitudes were greater in the dado than at other heights in all the vertical cross-sections. This lower part of the wall exhibited areas with greater or lesser intermediate moisture content and areas with no reflections (cross-sections 4 and 9, Figure 10) at heights under 1 m.

The radargram for survey profile 1 revealed the presence of moisture in some points around the confessional, most conspicuously in the dado. This finding was consistent with the saturation (RH in the 95 % to 100 % range) detected by the sensors in the preliminary monitoring campaigns [22]. As a rule, moisture content was greater around the confessional in the lower areas of the wall (profiles 1, 2 and 4, Figure 4).

b) South wall, horizontal cross-sections

Substantial differences were observed among the horizontal cross-sections for the south wall (Figure 11) depending on whether they were on (profile 12, 1.0 m), above (profile 13, 2.0 m) or below (profile 11, 0.0 m) the moisture front (see Figure 4).

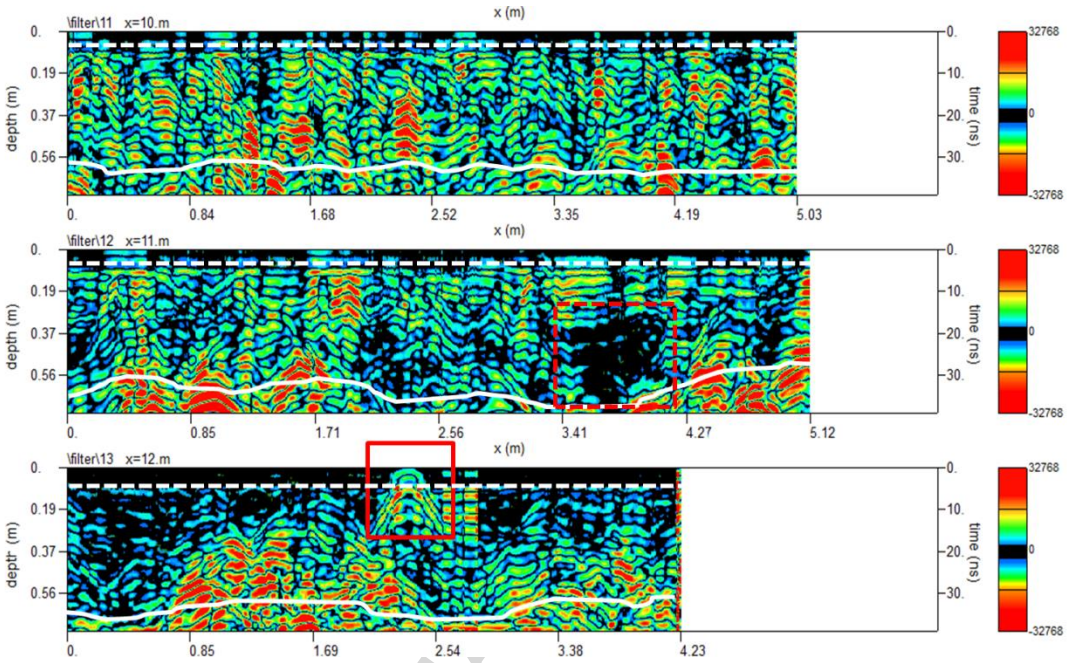

Figure 11. Horizontal radargrams on the south wall of the church; solid red outline: electrical wire; dashed white line: inward boundary of shallow mortar layers; solid white line: reflection indicating outside surface of wall

A high moisture content was observed in the plaster and cement mortar, with no reflections in these shallow layers in any of the cross-sections. Reflection amplitudes were generally similar for the profile 11 and 12 cross-sections (Figure 11), with a few areas with greater amplitude in 11 attributable to the dado and cavities in the dolostone. The moisture composition in the profile 12 cross-section was less uniform along the moisture front. The areas lacking reflections (dashed red lines, Figure 11), which are indicative of a high moisture content, delayed the reflection denoting the outside surface of the wall. Nonetheless, the cross-section for profile 13 exhibited reflections with very large amplitudes at depths of 0.37 m to 0.56 m, denoting lower moisture content due to solar radiation, as this profile was located above the moisture front. This cross-section also contained a reflection in the shallowest layers (solid red outline in Figure 11) at a distance of around 2.2 m attributable to an electrical socket that feeds power to one of the church lamps.

c) North wall, vertical cross-sections

Figure 12 shows the radargrams for some of the north wall vertical survey profiles. Unlike the south façade, the north wall exhibited no media differences, despite its 0.6 m high rubblestone dado, which is compositionally comparable to the stone masonry on the rest of the façade.

In the cross-section for the profile that concurred with the electrical resistivity profile (\bandpass\survey_21, Figure 12), the GRP findings showed that the reflection denoting the outside surface of the wall (white line) was deeper in the shallowest 0.50 m than in the rest of the cross-section. In other words, the wave travelled more slowly (two-way time around 18 ns) in those first few centimetres, indicating the presence of a higher moisture content there. The two-way times recorded here were similar to the times observed for the moisture front observed at a height of 1.0 m to 1.5 m on the south wall (Figure 10). This was consistent with the electrical conductivity meter readings for that wall, which detected the highest moisture range, with values of 60 % to 95 %, at a height of 1.30 m to 1.40 m. On the north wall, heights of under 0.5 m (dado), and occasionally and randomly up to 1.5 m also exhibited moisture in this range.

Variable phenomena were detected in the shallowest layers in the aforementioned cross-section, while amplitudes were smaller at heights of just under 2 m, which concurred with the minimum resistivities observed with ERT (Figure 9a)). Despite the large amplitudes in the area around 1.35 m, the two-way time for the respective reflection was greater. That finding was consistent with the ERT resistivity readings for the intermediate heights: 200 Ω to 300 Ω (Figure 9a)).

Although this was the cross-section for the profile that concurred with the site of the ERT readings, all the other vertical cross-sections of the north wall were also studied. That analysis showed that the distribution of high moisture content differed from cross-section to cross-section on the north wall as well as between these radargrams and the south wall radargrams. In light of Figure 12, cross-sections 18, 19 and 26 (Figure 12) acquired particular significance. In all three, scant reflections were detected at heights of over approximately 1.4 m, the areas most representative of the high moisture content in the wall. This paucity of reflections and the small amplitude of the few detected might be

interpreted to attest to wave attenuation by the high moisture content in the shallowest layers or alternatively to the presence of moisture farther into the wall. The latter cannot be ruled out, in light of the large areas on the outer façade affected by damp (Figure 6b)).

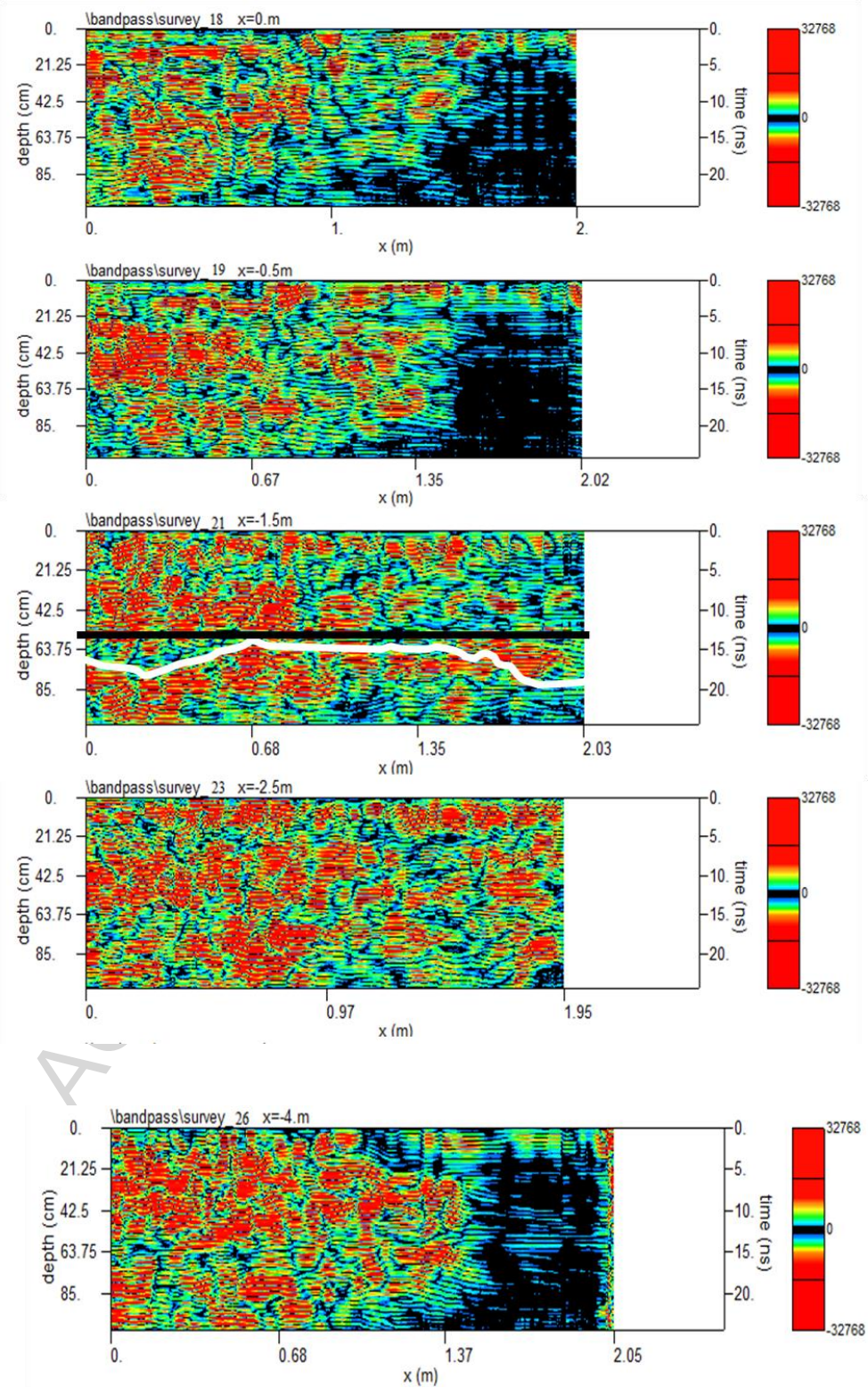

Figure 12. Radargram for the vertical profile that coincided with the electrical resistivity profile on the north wall of the church; solid black line: outside surface of wall; solid white line: reflection indicating outside surface of wall

Figure 12 shows a difference in wave behaviour between the moister layers closest to and the dryer layers farthest from the surface (>0.20 m), where interspersed larger amplitudes were observed. The electrical resistivity readings (Figure 9a)) at the depth reached with that technique, in turn, were upward of 800 Ω at heights of over 1.4 m. The inference to be drawn from these two findings is that in this medium and this cross-section, GPR detected and distinguished between moist and dry areas (Figure 12). Therefore, in the cross-sections with scant reflections at heights of over 1.4 m, moisture was interpreted to extend to the outside of the wall. That interpretation was supported by the surface moisture detected by electrical conductivity in this area (Figure 5). Evidence was also found for the heavy impact of surface water leakage in these upper areas, which penetrated through to the shallowest indoor layers (<0.20 m) where saturation had been detected by wireless sensors [25]. High moisture content was observed along the wall exteriors in some cross-sections.

d) North wall, horizontal cross-sections

As shown in Figure 13, which reproduces the radargrams for the horizontal profiles on the north wall, the highest moisture content in deep layers was detected in the cross-section for profile 30 (2.0 m), confirming the hypothesis established on the grounds of the ERT findings to the effect that the origin of the damp was rainwater leakage from the upper levels. The cross-section for the lowest height profile (28) exhibited a wave amplitude distribution visibly similar to the pattern observed on the south wall.

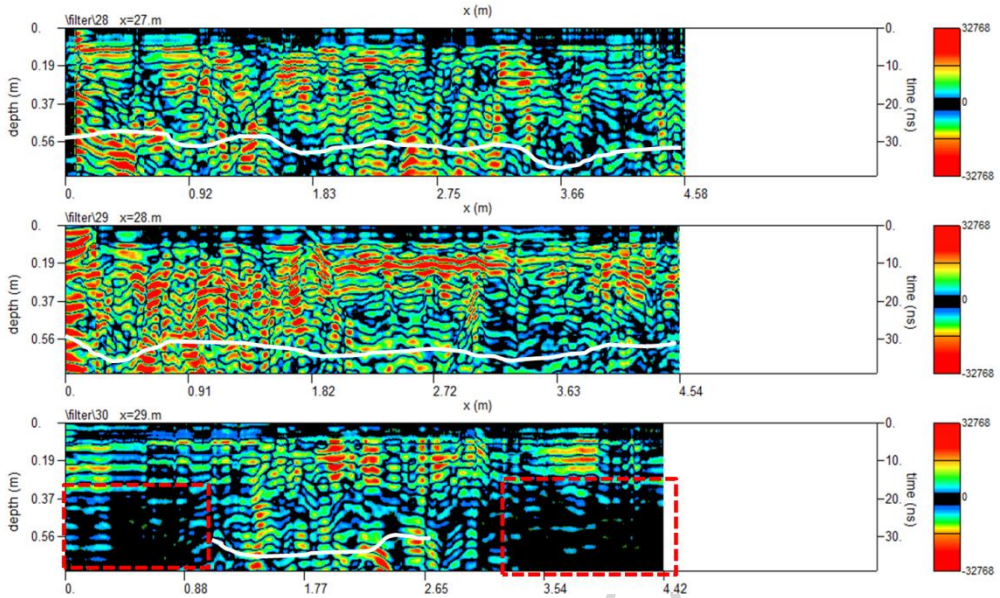

Figure 13. Horizontal radargrams for the north wall of the church; dashed red outline: area with no reflections; solid white line: reflection indicating outside surface of wall

Due to the constraints on physical access with the GPR instruments, the floor profile closest to the wall did not concur exactly with the profile analysed with ERT, although they were within 0.1 m to 0.2 m of one another. The GPR profile was sited over stone pavers.

e) South side floor cross-sections

Figure 14 shows some of the floor cross-sections analysed on the south side of the church. In the cross-sections for profiles 15 and 16 (Figure 4), a change from a more to a less compact medium was detected at a depth of around 0.37 m, where the infill gave way to the original soil. A few reflections attributed to the pavers were observed in the profile 15 cross-section, which had no underlying structures, according to the church staff. The change from infill to soil appeared at a depth of 0.19 m in the cross-section for profile 17, sited at a farther distance from the wall. The cross-section for profile 14, which was perpendicular to the other cross-sections in Figure 14, also exhibited a reflection denoting a change of medium, represented by a white line present at a depth of 0.37 m in the profile 15 and 16 cross-sections and at 0.19 m in the cross-section for profile 17.

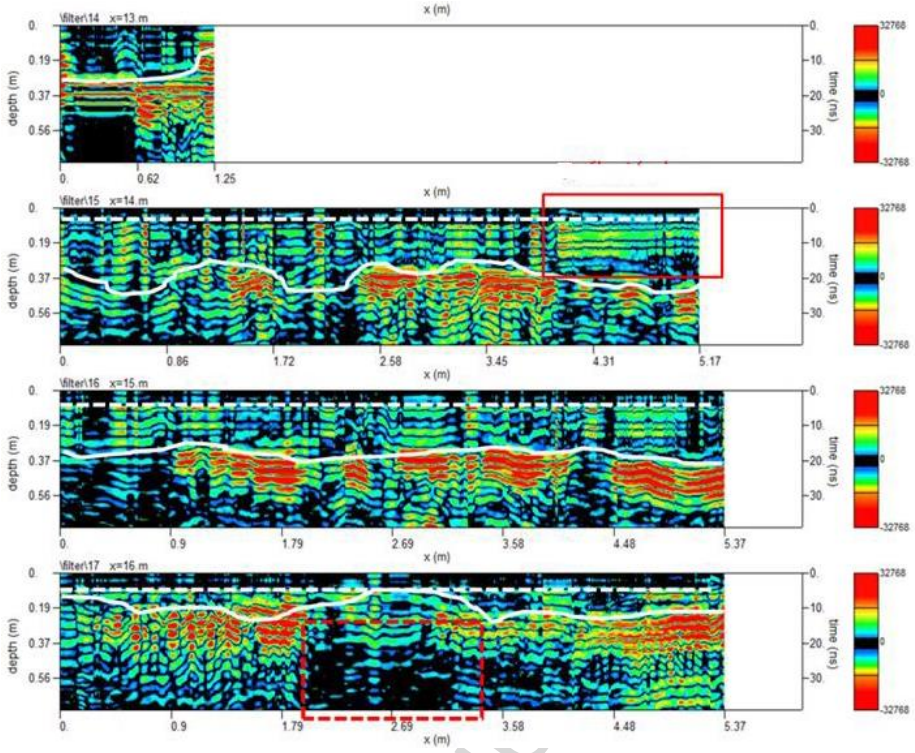

Figure 14. Under-floor radargrams alongside the south wall of the church; solid red outline: pavers; solid white line: change of medium; dashed white line: lower boundary of upper-most mortar layers severely affected by damp

f) North side floor cross-sections

Figure 15 shows some of the wave transmission findings for the under-floor cross-sections alongside the north wall. Profile 31 was closest to the ERT profile (Figure 4). Overall, large areas with no reflections were observed at depths of over 0.37 m, where the medium was observed to change, as it did under the floor along the south wall. On this north side, the reflection denoting the change of medium also appeared at 0.19 m in the cross-section for profile 33, the one farthest from the wall. The GPR findings likewise confirmed that the original soil contained more moisture along the north than along the south wall. In the former, larger areas with scant reflections were found primarily in the cross-sections closest to the wall (profiles 31 and 32), which was consistent with the results of surface monitoring in this area (Figure 5).

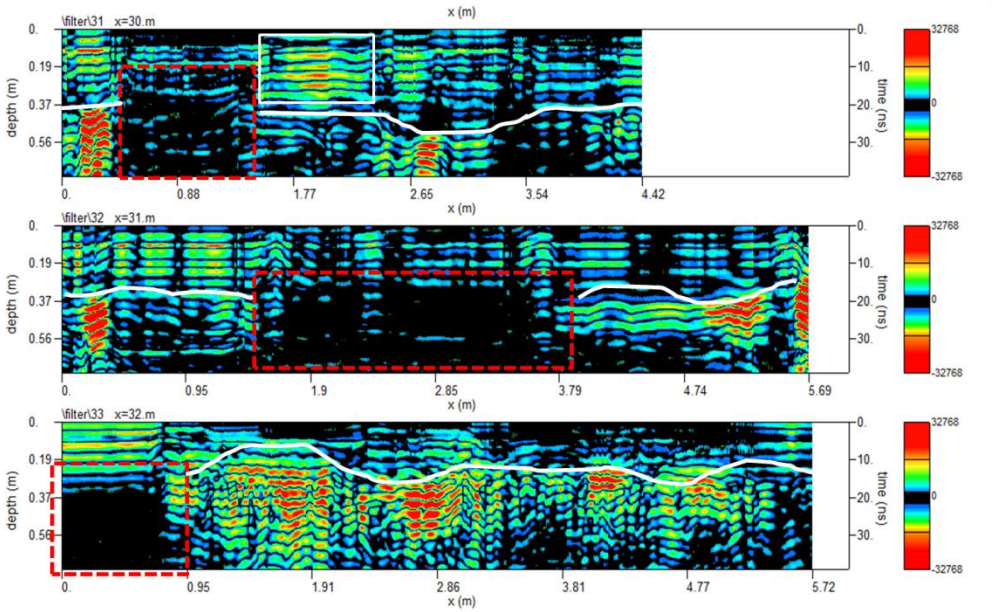

Figure 15. Under-floor radargrams alongside the north wall of the church; dashed red outline: area with no reflections; solid white line: change of medium; solid white outline: pavers

4. DISCUSSION AND CONCLUSIONS

This study involved the joint use of non- or minimally destructive techniques to determine the origin of damp affecting a building. Their range of observation was observed to differ.

The main pillars on which the viability and range of each technique rest are affordability and accessibility or ease of use on the one hand and on the other, the depth to which acceptably precise results are obtained.

4.1. Comparison of affordability and accessibility

This section compares the price and ease of use of the monitoring techniques deployed. An affordability scale of 0 to 5 was defined, in which 0 was the least and 5 the most expensive technique on the market at this writing. An accessibility score of 0 was attributed to techniques requiring a good command of the subject to use the equipment and correctly interpret the results, whereas a score of 5 was attributed to techniques in

which equipment operation calls for no prior knowledge and interpretation of the results is simple and intuitive. Comparison results were:

- Dataloggers/Electrical conductivity meter: affordablity (1) & accessibility (5).
- IR: affordablity (3) & accessibility (4).
- WSN: affordablity (2) & accessibility (3).
- ERT: affordablity (5) & accessibility (2).
- GPR: affordablity (4) & accessibility (1).

Data loggers and electrical conductivity meters are the most inexpensive and accessible instruments, for they require no extensive knowledge to interpret the results. Electrical conductivity meters provide fuller information on wall surface conditions. Nonetheless, new low-cost IR thermographic products are being launched on the market [54-56], raising the affordability of these likewise intuitively operated instruments, which deliver the most readily interpreted results. Wireless sensor networks, in turn, feature the best price-ease of use ratio, whilst ERT and GPS are the costliest and least accessible techniques from the standpoint of understanding their operating principles and exploiting the results, which call for professional expertise.

4.2. Comparison of scope and precision of results

a) Electrical conductivity meter, IR and WSN

Electrical conductivity meters and infrared thermography deliver rough estimates of the extent of damp on wall surfaces, furnishing qualitative information on the areas where depth studies should be undertaken using techniques such as ERT or GPR or where long-term WSN monitoring sensors should be positioned. For sub-surface inspection, the other study techniques used here are required. In this study wireless sensor networks proved to be very useful, for they provide for long-term monitoring at a low cost, either after a preliminary electrical conductivity or thermography analysis or to determine variability in a given number of points after ERT or GPR surveys.

b) ERT and GPR

When sub-surface conditions need to be monitored in an area where the number of reading points is larger than could be feasibly instrumented with WSN, the techniques of choice are ERT or GPR.

The depth reached with GPR can be equalled by ERT by increasing the distance between electrodes, although to the detriment of the resolution delivered. When the purpose is to distinguish between areas with widely varying moisture contents, ERT is more precise. In this study, the absence of GPR reflections in areas with a high moisture content in the shallowest layers was found to distort the results for deeper and dryer layers.

Another conclusion that can be drawn from the present findings is that the range of changes in moisture content that can be detected with GPR, expressed in terms of electrical resistivity values (Figures 12 and 13), can be delimited. On a qualitative scale (high, intermediate, low), high moisture contents would be associated with resistivity values of under 20 Ω. In media with very moist shallow layers, GPR reflections could be discerned at deeper layers when ERT readings fluctuated between around 100 Ω and 500 Ω or greater.

c) Conclusions

The ERT and GPR cross-sections for the same profile on the south wall identified a moisture front at around mid-height of the area analysed (1.0 m to 1.5 m), while GPR detected a change in medium between the dado and the masonry in the rest of the wall. The moisture content was so high at the front in the surface mortar layers that the wave was practically attenuated, with barely any reflections recorded along the outside of the wall. Under these conditions, the reflection denoting the outside surface of the wall exhibited a longer delay. ERT, however, showed that at a depth of 0.20 m from the indoor surface, resistivity values rose and the moisture content declined due to the effect of solar radiation on the exterior brick and rubblestone masonry. The high moisture content in the centimetres closest to the indoor wall surface observed with ERT and GPR in areas around the confessional at heights of under 0.5 m were also detected by the sensor networks, which recorded saturation in these areas [22].

The GPR cross-section for the profile on the north wall that concurred with the ERT profile on that wall showed no medium change, inasmuch as the dado is compositionally similar to the large quartzite rubble masonry found in the rest of the wall. Even though this was among the most uniform cross-sections, however, higher moisture content was observed in the shallowest layers at heights of approximately 1.2 m and over. A reflection denoting changes in moisture also appeared, with minimum two-way times at around 1.3 m and in the upper areas near the 2.0 m survey limit. In the cross-section of the wall surveyed with both techniques, GPR was able to distinguish changes in moisture content (where the ERT readings varied from 100 Ω to 800 Ω). Very high moisture content was also recorded inside the wall in other vertical cross-sections at heights of over 1.3 m to 1.5 m. These findings were consistent with the electrical conductivity meter results (Figure 8) and the infrared thermography data for façade exteriors (Figure 9), providing support for the complementarity of thermography and GPR results.

An analysis of the findings delivered by the techniques used showed that the highest moisture content was detected at an intermediate height on the south wall (1.0 m to 1.5 m, between the stone ashlar/rubble masonry dado and the rest of the wall, where brick masonry flanks rubblestone panels) and at higher elevations on the north wall. The latter was attributed to the greater sorptivity of the clay filler inside the north wall and the mortar surfacing and fill in its large rubblestone panels.

A qualitative comparison of resistivities revealed that moisture was greatest in the shallowest layers in the upper part of the north wall, with very high values also recorded at mid-height. The main construction materials were also detected. The layers most severely affected by the moisture content were the clay fillers and the plaster, lime and cement mortar surfacing. On the south wall the moisture content distribution by height exhibited very high resistivity values (indicative of very low moisture content) in the deeper layers at higher elevations, attributed to the effect of solar radiation (Figure 12). Moisture content was very high in the shallowest indoor layers, primarily at around 0.5 m and 1.5 m, where the electrical conductivity meter detected surface moisture fronts. The presence of these fronts inside the wall was subsequently confirmed by the wireless network. The resistivity value ranges were lower for the north than for the south wall cross-sections, indicating that the moisture content was higher in the former, generally speaking.

GPR proved to be the most accessible and efficient technique for studying the under-floor profiles, followed by ERT, which called for more elaborate instrumentation. The floor radargrams were fairly similar on the north and south sides of the church, whilst the lowest resistivity values (highest moisture content), recorded for the shallowest layer on the south side, were attributed to capillary water absorption. Low resistivity was also observed on the north side at somewhat deeper layers than in the south. The resistivity ranges were similar, with the highest values found at depths of 0.1 m to 0.2 m. Resistivity was highest (moisture lowest) at around mid-length of the floor profile monitored (0.8 m to 1.6 m) through to the lowest depth monitored, although on the south side areas with higher values were also observed at a depth of around 0.4 m, denoting the presence of less uniform filler materials.

The conclusion drawn from the joint use of the two techniques was that the origin of the damp was the rise of capillary water on the north and south sides, intensified on the north by rainwater leakage. Solar radiation-governed wet-dry and salt dissolution-crystallisation-rehydration cycles inside the south wall favour decay in this wall, which is visible from inside the church.

In light of these findings, the guidelines to be followed to stay the effects of decay consist in reducing capillary rise. That would entail replacing the cement layer with a mortar more permeable to water vapour to favour evaporation. It would also be advisable to prevent water inflow from outside the church by building a protective shield or an air space to ventilate the foundations. Rainwater leakage should be remedied by modifying the eaves or installing gutters to re-channel surface water, particularly on the north façade.

In addition to this direct action, indoor microclimatic conditions and with them wall moisture content should also be monitored. Wireless sensors installed to alert to rises in moisture should be combined with a system to automatically ventilate the church and help keep its walls dry.

Acknowledgments

The loan of instruments and equipment by the Archaeometry and Archaeological Analysis Research Support Centre (Complutense University of Madrid, UCM) and the Petrophysics Laboratory (Geosciences Institute, National Research Council-UCM), arranged through the

Moncloa Campus of International Excellence (UCM -Technical University of Madrid, UPM), is gratefully acknowledged. The authors wish to thank the Diocese of Alcalá for its cooperation throughout. The present study was funded under projects CGL2011- 27902, GEOMATERIALES 2 (S2013/MIT-2914). The manuscript was edited by Margaret Clark, professional translator and English language science editor.

References

1. Martínez Garrido MI (2015) Aportación de la monitorización mediante redes de sensores y técnicas no invasivas para la conservación preventiva del Patrimonio, 440p. (Doctoral Thesis). School of Telecommunications Engineering (ETSIST), Technical University of Madrid (UPM).

2. Fertitta G, Di Stefano A, Fiscelli G, Giaconia CG (2009) An Embedded Datalogger with a Fast Acquisition Rate for In-Vehicle Testing and Monitoring. Conti M, Orcioni S, Grammatikakis MD. PROCEEDINGS OF THE SEVENTH INTERNATIONAL WORKSHOP ON INTELLIGENT . , pp 105-110.

3. McCullagh JJ, Galchev T, Peterson RL, Gordenker R, Zhang Y, Lynch J, Najafi K (2014) Long-term testing of a vibration harvesting system for the structural health monitoring of bridges. Sensors and Actuators A: Physical 217:139-150. doi: http://dx.doi.org/10.1016/j.sna.2014.07.003.

4. Abu-Zeid N, Botteon D, Cocco G, Santarato G (2006) Non-invasive characterisation of ancient foundations in Venice using the electrical resistivity imaging technique. NDT E Int 39:67-75. doi: 10.1016/j.ndteint.2005.06.007.

5. Martinho E, Alegria F, Dionisio A, Grangeia C, Almeida F (2012) 3D-resistivity imaging and distribution of water soluble salts in Portuguese Renaissance stone bas-reliefs. Eng Geol 141–142:33-44. doi: http://dx.doi.org/10.1016/j.enggeo.2012.04.010.

6. Masini N, Nuzzo L, Rizzo E (2007) GPR investigations for the study and the restoration of the rose window of Troia Cathedral (southern Italy). Near Surface Geophysics 5:287-300.

7. Leucci G, Masini N, Persico R, Soldovieri F (2011) GPR and sonic tomography for structural restoration: the case of the cathedral of Tricarico. Journal of Geophysics and Engineering 8:S76-S92. doi: 10.1088/1742-2132/8/3/S08.

8. Grossi D, Lama EAD (2015) Ultrasound technique to assess the physical conditions of the Monument to Ramos de Azevedo, city of São Paulo, Brazil. Rem: Revista Escola de Minas 68:171-176. doi: 10.1590/0370-44672015680017.

9. Mercuri F, Cicero C, Orazi N, Paoloni S, Marinelli M, Zammit U (2015) Infrared Thermography Applied to the Study of Cultural Heritage. Int J Thermophys 36:1189-1194. doi: 10.1007/s10765-014-1645-x.

10. Cadelano G, Bison P, Bortolin A, Ferrarini G, Peron F, Girotto M, Volinia M (2015) Monitoring of historical frescoes by timed infrared imaging analysis. Opto-Electronics Review 23:100-106. doi: 10.1515/oere-2015-0012.

11. Bradley S (2005) Preventive conservation research and practice at the British Museum. Journal of the American Institute for Conservation 44:159-173.

12. Barraca, N., Almeida, M., Varum, H., Almeida, F., Senos Matias, M. (2016) A case study of the use of GPR for rehabilitation of a classified Art Deco building: The InovaDomus house. Journal of Applied Geophysics 127:1–13.

13. Paoletti D, Ambrosini D, Sfarra S, Bisegna F (2013) Preventive thermographic diagnosis of historical buildings for consolidation. Journal of Cultural Heritage 14:116-121.

14. Walker R, Pavia S, Dalton M (2016) Measurement of moisture content in solid brick walls using timber dowel. Mater Struct 49:2549-2561. doi: 10.1617/s11527-015-0667-6.

15. Sass O, Viles HA (2010) Two-dimensional resistivity surveys of the moisture content of historic limestone walls in Oxford, UK: implications for understanding catastrophic stone deterioration. Limestone in the Built Environment: Present Day Challenges for the Preservation of the Past 331:237-249. doi: 10.1144/SP331.22.

16. Garcia Morales S, Lopez González L, Collado Gómez A (2012) Metodología de inspección higrotérmica para la determinación de un factor intensidad de evaporación en edificios históricos. Informes de la Construcción 64:69-78.

17. D'Agostino D (2013) Moisture dynamics in an historical masonry structure: The Cathedral of Lecce (South Italy). Build Environ 63:122-133. doi: 10.1016/j.buildenv.2013.02.008.

18. Lerma C, Mas A, Gil E, Vercher J, Penalver MJ (2014) Pathology of building materials in historic buildings. Relationship between laboratory testing and infrared thermography. Materiales De Construccion 64:e009. doi: 10.3989/mc.2013.06612.

19. Fort R, Alvarez de Buergo M, Perez-Monserrat EM, Gomez-Heras M, Jose Varas-Muriel M, Freire DM (2013) Evolution in the use of natural building stone in Madrid, Spain. Quarterly Journal of Engineering Geology and Hydrogeology 46:421-429. doi: 10.1144/qjegh2012-041.

20. Varas-Muriel MJ, Martínez-Garrido MI, Fort R (2014) Monitoring the thermal–hygrometric conditions induced by traditional heating systems in a historic Spanish church (12th–16th C). Energy Build 75:119-132. doi: http://dx.doi.org/10.1016/j.enbuild.2014.01.049.

21. Fort R, Varas MJ, Alvarez de Buergo M, Freire DM (2011) Determination of anisotropy to enhance the durability of natural stone. Journal of Geophysics and Engineering 8:132-144.

22. Martínez-Garrido MI, Aparicio S, Fort R, Anaya JJ, Izquierdo MAG (2014) Effect of solar radiation and humidity on the inner core of walls in historic buildings. Construction and Building Materials 51 51:383-394.

23. Varas-Muriel MJ, Fort R, Martínez-Garrido MI, Zornoza-Indart A, López-Arce P (2014) Fluctuations in the indoor environment in Spanish rural churches and their effects on heritage conservation: Hygro-thermal and CO2 conditions monitoring. Build Environ 82:97-109. doi: http://dx.doi.org/10.1016/j.buildenv.2014.08.010.

24. General Electric Company (2015) GE Measurement&Control, Surveymaster Moisture Meter. http://www.ge-mcs.com/en/moisture-and-humidity/moisture-meters/surveymaster.html. Accessed 01/152015.

25. Martínez Garrido MI, Gómez Heras M, Fort R, Varas Muriel MJ (2014) Monitoring moisture distribution on stone and masonry walls. Rogerio-Candeleda MA. Science, Technology and Cultural Hetitage for the Conservation of Cultural Heritage. , CRC Press/Balkema, pp 35-40.

26. Golden Software Surfer 12. http://www.goldensoftware.com/products/surfer. Accessed 01/152015.

27. Maxim Integrated Products I (2013) DS1923 Maxim Integrated. http://datasheets.maximintegrated.com/en/ds/DS1923.pdf. Accessed 01/152015.

28. Maxim Integrated (2016) OneWireViewer. https://www.maximintegrated.com/en/products/ibutton/software/1wire/OneWireViewer.cfm;. Accessed 03/092016.

29. Smartmote Smartmote Monitoring & Testing.

30. Gnawali O, Fonseca R, Jamieson K, Kazandjieva M, Moss D, Levis P (2013) CTP: An Efficient, Robust, and Reliable Collection Tree Protocol for Wireless Sensor Networks. Acm Transactions on Sensor Networks 10 (1). doi: 10.1145/2529988.

31. Bucur D, Iacca G, Squillero G, Tonda A (2014) The impact of topology on energy consumption for collection tree protocols: An experimental assessment through evolutionary computation. Applied Soft Computing 16:210-222. doi: 10.1016/j.asoc.2013.12.002.

32. Martínez-Garrido MI, Fort R (2014) Sensing technologies for monitoring and conservation of cultural heritage: wireless detection of decay factors. Rogerio-Candeleda MA. Science, Technology and Cultural Heritage. , CRC Press/Balkema, pp 495-501.

33. Martínez-Garrido MI, Fort R (2016) Experimental assessment of a wireless communications platform for the built and natural heritage. Measurement 82:188-201. doi: http://dx.doi.org/10.1016/j.measurement.2015.12.036.

34. Martínez Garrido MI, Fort R (2015) Wireless communications platforms for built and natural heritage monitoring. Anonymous Sensing the Past: Geoscience and Sensing Technologies for cultural heritage. , Springer.

35. ANSI/IEC 60529 (2004) Degrees of Protection Provided by Enclosures (IP Code) (identical national adoption). , National Electrical Manufacturers Association.

36. Presuel-Moreno F, Liu Y, Wu Y- (2013) Numerical modeling of the effects of rebar presence and/or multilayered concrete resistivity on the apparent resistivity measured via the Wenner method. Constr Build Mater 48:16-25. doi: 10.1016/j.conbuildmat.2013.06.053.

37. GEOLOG2000 System- und Meßtechnik GEOLOG2000. http://www.geolog2000.de/geolog2000/index2000.html. Accessed 01/152015.

38. Cezar GD, da Rocha PLF, Buarque A, da Costa A (2001) Two Brazilian archaeological sites investigated by GPR: Serrano and Morro Grande. J Appl Geophys 47:227-240.

39. Zhao W, Forte E, Pipan M, Tian G (2013) Ground Penetrating Radar (GPR) attribute analysis for archaeological prospection. J Appl Geophys 97:107-117. doi: 10.1016/j.jappgeo.2013.04.010.

40. Lasaponara R, Leucci G, Masini N, Persico R (2014) Investigating archaeological looting using satellite images and GEORADAR: the experience in Lambayeque in North Peru. Journal of Archaeological Science 42:216-230. doi: http://dx.doi.org/10.1016/j.jas.2013.10.032.

41. Sala R, Tamba R, Garcia-Garcia E (2016) Application of Geophysical Methods to Cultural Heritage. Elements 12(1):19-25. doi: 10.2113/gselements.12.1.19.

42. Nuzzo L (2004) The contribution of GPR to investigate damages in the Crypt of the Cathedral of Otranto (Apulia, Italy).

43. Leucci G, Persico R, Soldovieri F (2007) Detection of fractures from GPR data: the case history of the Cathedral of Otranto. Journal of Geophysics and Engineering 4:452-461. doi: 10.1088/1742-2132/4/4/011.

44. Pérez-Gracia V, Caselles JO, Clapés J, Martinez G, Osorio R (2013) Non-destructive analysis in cultural heritage buildings: Evaluating the Mallorca cathedral supporting structures. NDT E Int 59:40-47. doi: http://dx.doi.org/10.1016/j.ndteint.2013.04.014.

45. Guadagnuolo M, Faella G, Donadio A, Ferri L (2014) Integrated evaluation of the Church of S. Nicola di Mira: Conservation versus safety. NDT E Int 68:53-65. doi: 10.1016/j.ndteint.2014.08.002.

46. Roch KH, Chwatal W, Bruckl E (2006) Potentials of monitoring rock fall hazards by GPR: considering as example the results of Salzburg. Landslides 3:87-94. doi: 10.1007/s10346-005-0026-8.

47. Masini N, Persico R, Rizzo E (2010) Some examples of GPR prospecting for monitoring of the monumental heritage. Journal of Geophysics and Engineering 7:190-199. doi: 10.1088/1742-2132/7/2/S05.

48. Leucci G, Masini N, Persico R (2012) Time-frequency analysis of GPR data to investigate the damage of monumental buildings. Journal of Geophysics and Engineering 9:S81-S91. doi: 10.1088/1742-2132/9/4/S81.

49. Ihamouten A, Le Bastard C, Boutet N, Villain G, Derobert X (2013) GPR characterization of water transfers in Tuffeau walls.

50. USRADAR INC. Subsurface Imaging Systems Ground penetrating radar (GPR) products: 1000 MHz cart systems. . Accessed 10/312014.

51. Pérez Gracia, María de la Vega (2001) Radar de subsuelo.Evaluación para aplicaciones en arqueología y en patrimonio histórico-artístico.

52. Ming-Chih L, Yu-Ming K, Kun-Fa L, Hui-Chi H (2009) A Study on the Technologies for Detecting Underground Water Level and Processing Image. International Journal of Applied Science and Engineering 7(1):61-68.

53. Biskup K, Lorenzo H, Arias P (2005) Aplicabilidad del radar de subsuelo para el estudio de la zona no saturada del suelo: ejemplos en ambientes arenosos costeros. Samper Calvete FJ, Paz González A. Estudios de la zona no saturada del suelo. , pp 197-204.

54. FLIR Systems Inc. (2016) FLIR ONE. http://www.flir.es/flirone/content/?id=62912. Accessed 03/092016.

55. Seek Thermal Inc. (2016) Seek Thermal. http://www.thermal.com/. Accessed 03/092016.

56. Caterpillar (2016) Cat S60 Smartphone. http://www.catphones.com/en-gb/phones/s60-smartphone. Accessed 03/092016.

Highlights

- A complete study by NDT for moisture control in the cultural heritage is developed
- Evaluation methodology with GPR, ERT, WSN, IRT and contact hygrometry.
- Observation ranges were inter-related to identify decay in construction materials
- Advantages and drawbacks of each instrumental method are described.
- Innovative applications of geophysical techniques for moisture control.